High precision batch mode micro-electro-discharge machining of metal alloys using DRIE silicon as a cutting tool

2013 J. Micromech. Microeng. 23 095026

(http://iopscience.iop.org/0960-1317/23/9/095026)

J. Micromech. Microeng. **23** (2013) 095026 (11pp) doi:10.1088/0960-1317/23/9/095026

High precision batch mode micro-electro-discharge machining of metal alloys using DRIE silicon as a cutting tool

Tao Li[1,3], **Qing Bai**[2] **and Yogesh B Gianchandani**[1]

[1] Center for Wireless Integrated MicroSensing and Systems (WIMS[2]), University of Michigan, Ann Arbor, MI, USA
[2] Molecular Separations Laboratory, Agilent Research Laboratories, Santa Clara, CA, USA

E-mail: litz@umich.edu

Received 26 February 2013, in final form 26 July 2013
Published 28 August 2013
Online at stacks.iop.org/JMM/23/095026

Abstract
This paper reports recent advances in batch mode micro-electro-discharge machining (μEDM) for high precision micromachining of metal alloys such as stainless steel. High-aspect-ratio silicon microstructures with fine feature sizes formed by deep reactive ion etching are used as cutting tools. To machine workpiece features with widths $\leqslant$10 μm, a silicon dioxide coating is necessary to passivate the sidewalls of the silicon tools from spurious discharges. In the machined workpieces, a minimum feature size of $\approx$7 μm and an aspect ratio up to 3.2 are demonstrated by the batch mode μEDM of stainless steel 304 and titanium (Grade 1) substrates. Machining rates up to $\approx$5 μm min^{-1} in feature depth are achieved in batch mode micromachining of typical microfluidic structures, including arrays of channels and cavities of different sizes. The machined features are uniform across a die-scale area of 5 $\times$ 5 mm^2. Other machining characteristics are also discussed.

(Some figures may appear in colour only in the online journal)

1. Introduction

Stainless steel and other metal alloys are attractive as structural and packaging materials in microsystems because of superior mechanical strength, chemical resistance and other desirable properties. For example, stainless steel has been used for smart stents [1], micro-packages for implantable devices [2], microfluidic devices for gas chromatography [3], high power micro-relays [4] and pressure sensors for oil-exploration [5]. Alloys of titanium have been used for packaging micromachined sensors for harsh environments [6, 7], and for *in vivo* applications [8]. Metglas^{TM}, a collection of magnetic alloys of Fe, Ni, and other metals, is used commercially in anti-theft tags [9], and has been explored for microsensing applications [10].

The micromachining of metal alloys, however, is typically not amenable to traditional lithography-compatible microfabrication approaches. Mechanical processes like micromilling, microdrilling, etc, are effective on most varieties of alloys but the machining performance greatly depends on the mechanical properties of the workpiece material. The smallest machined features are typically larger than a few tens of microns [11]. These processes are also serial, resulting in lower throughput for complicated patterns. In addition, tool wear can contribute to non-uniformity in the machined parts. Laser machining and laser-induced wet-chemical etching can achieve features $<$10 μm but are also serial processes [12]. Electrochemical micromachining (ECM) has been used in both serial and batch modes, with resolution $<$20 μm. However, not all the metals contained in an alloy are etched at the same rate. Moreover, difficulty in electrolyte handling (e.g., for titanium alloys) and insoluble byproducts (e.g., for tungsten carbide)

[3] Author to whom any correspondence should be addressed.

add to the complications of using ECM for these materials [11, 13]. Wet-chemical etching is typically limited to an aspect ratio <0.5 due to lateral undercutting. It also requires different etchants for different metal alloys [14].

Micro-electro-discharge machining (μEDM) can complement other technologies in terms of resolution and throughput. It can be used to make microstructures from any electrically conductive material, including any metal alloy, with feature sizes down to 5 μm [11, 15]. This approach utilizes sequential spark microdischarges between a cutting tool (cathode) and a workpiece (anode) while both are immersed in dielectric oil. Material removal occurs by melting and evaporation with the thermal energy released during the discharge. A resistor–capacitor circuit precisely controls the discharge timing and the energy of each spark, allowing micro-scale features to be machined. The process can be applied in either serial or batch mode. In the serial (or milling) mode, a single rotating tool is scanned or scrolled across a workpiece surface for machining, giving limited throughput especially for complex patterns [15]. Batch mode μEDM (die sinking) uses a tool electrode with pre-formed patterns to machine multiple features in parallel [16].

High-aspect-ratio microstructures with high precision in both geometry and location are necessary on the batch mode μEDM tool to achieve high precision machining. Traditionally the tools in die-sinking EDM are prepared by milling of copper or graphite. We previously reported a batch mode μEDM process that uses lithographically-defined, electroplated copper structures as cutting tools [17]. By using x-ray lithography [18], it was possible to batch fabricate tools that have 20 μm feature width and height exceeding 300 μm. However, there is significant complexity in electroplating high-aspect-ratio structures. As the aspect ratio of the plating mold increases, it becomes more challenging to maintain uniformity in the electroplating current, and the chemical integrity of the electroplating solution is compromised by local variations in flow characteristics. It also becomes more difficult to eliminate voids and to ensure that the seed layer is clear of photoresist and air bubbles at all plating sites. Moreover, it has been observed that electroplated copper structures soften and are prone to significant deformation and recasting into a mushroom shape during batch mode μEDM, degrading machining precision and surface quality, machining depth and tool wear [19, 20]. Also within the scope of batch mode μEDM, 'reverse EDM' uses a planar tool with through holes and/or other negative patterns to machine posts and/or other positive features [21–23]. Micro-wire electro-discharge machining (WEDM) has been used to machine an array of square rods using the length of a thin wire as the tool [24]. An array of rotary disc electrodes has been used as a tool to machine parallel array of straight micro-slits with μEDM [25]. This method and WEDM do not easily accommodate arbitrary shapes to be machined in parallel.

This paper reports the use of silicon as a cutting tool in batch mode μEDM[4]. The usefulness of Si in this role was anticipated in a patent [27], for which preliminary results were obtained using wet-etched Si. This paper reports the first results obtained with high-aspect-ratio Si cutting tools that are fabricated by deep reactive ion etching (DRIE). With the development and maturity of the DRIE technology, Si microstructures with high aspect ratio and ultra-fine feature sizes can be readily made. The process details are described in section 2. Die-scale batch-fabrication of several typical forms of microstructures for microfluidic devices is demonstrated on stainless steel 304 (SS304), SS316, and titanium (Grade 1) substrates, and the results are reported in section 3. The precision that can be achieved with Si cutting tools is assessed. Other process characteristics are also described and are followed by discussion in section 4.

[4] Portions of this paper appear in conference abstract form in [26].

2. Process description

Batch mode μEDM using Si as a tool material can benefit from the established DRIE technology in preparing high-aspect-ratio tool microstructures, achieving high precision in both geometries and positioning of the tool features.

2.1. Silicon as a tool material for μEDM

During the EDM process, both the tool and the workpiece are subjected to spark erosion, resulting in tool wear in addition to material removal from the workpiece. For lower tool wear, the preferred materials have high melting points, high thermal conductivity, high specific heat, and low electrical resistivity [28]. A numerical value, named the erosion resistance index (E_I), has been defined to indicate how resistant a material is to the spark erosion process [29, 30]. It is given by:

$$E_I = kcT_m^2 \tag{1}$$

where k is the thermal conductivity in W (m K)$^{-1}$, c is the specific heat in J (kg K)$^{-1}$, and T_m is the melting point in Kelvin. Although the index E_I is not comprehensive and the effect of its quantitative value is arguable, it provides a first order assessment of the suitability of a material for a μEDM tool. Typically materials with higher E_I tend to generate less wear when used as tools in regular machining conditions. In conventional macro-scale EDM, copper, graphite, tungsten and its alloys are most commonly used tool materials [28]. At the micro-scale, tungsten wire is the most popular choice of materials for tool electrodes in serial mode μEDM, while electroplated copper has been used for batch mode μEDM [15, 31, 32]. The relevant properties and the calculated E_I indices of these materials are listed in table 1 and compared with those of p^{++} Si, SS304 and Ti (Grade 1). The E_I index for Si is smaller but comparable to those of other common tool materials[5], and is several times larger than that of SS304 and Ti (Grade 1). Although it is not the best option for tool electrodes in terms of material properties, the major advantage of using Si as a tool material for batch mode μEDM is that there are readily available, matured processing technologies to generate high precision, high-aspect-ratio Si microstructures, such as DRIE [33].

[5] [30] presents an E_I index of Si that is 300–400 times smaller than those of tungsten and copper, without fully disclosing raw values of the relevant material properties. A discrepancy in the units in the listed values was also found.

Table 1. Comparison of properties of p^{++} Si and other commonly-used μEDM tool electrode materials. Properties of SS304 and Ti (Grade 1) workpiece materials are also listed for comparison.

	p^{++} silicon [37–39]	Copper [40, 41]	Graphite [40, 41]	Tungsten [41, 42]	SS304 [40, 42]	Ti (Grade 1) [40, 43]
Melting point (°C)	1412	1084	3650	3422	1400–1455	1670
Thermal conductivity ($W(m\ K)^{-1}$)	80–130	401	25–470	173	16.2	16.0–16.3
Specific heat ($J\ (kg\ K)^{-1}$)	700	380	710–830	130	500	520–540
Electrical resistivity (Ω cm)	5×10^{-3}	1.65×10^{-6}	$0.5–3 \times 10^{-3}$	5.49×10^{-6}	72×10^{-6}	$45–56 \times 10^{-6}$
Calculated E_I index ($10^{11} J^2\ (m\ s\ kg)^{-1}$)	1.59–2.58	2.81	2.73–60	3.07	0.23–0.24	0.31–0.33

Note: All values are at room temperature.

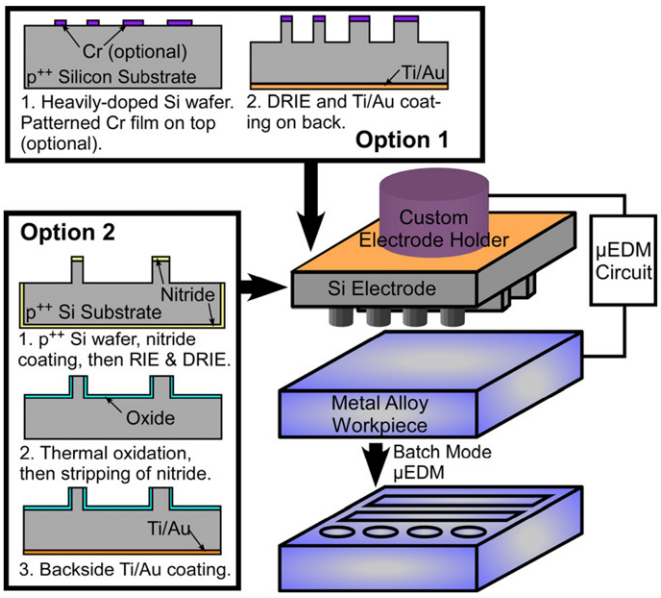

Figure 1. Concept of batch mode μEDM for metal alloy workpiece using DRIE Si tools. Two options are illustrated for tool preparation. Option 1 is a simpler sequence for regular applications with bare Si microstructures. (An optional Cr coating can be formed on the top surfaces.) Option 2 allows addition of a SiO_2 passivation layer on the sidewalls of the Si microstructures for protection of tool structures especially at small feature sizes <10 μm.

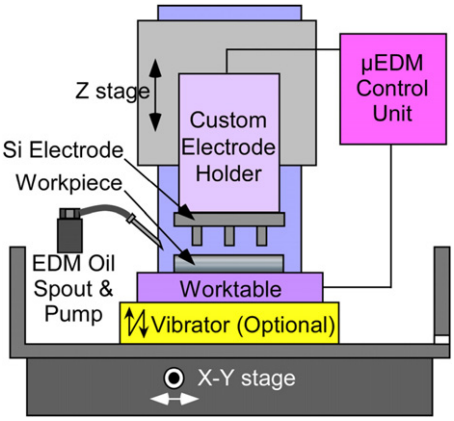

Figure 2. SmalTec EM203 μEDM machine adapted for batch mode micromachining of metal alloy workpiece with Si tools.

2.2. Process details

The approach for batch mode μEDM using DRIE Si tools is shown in figure 1. In one option, the preparation of Si tools starts with a heavily boron-doped, p^{++} Si wafer (e.g., 0.001–0.005 Ω cm resistivity). A layer of Cr (100–500 nm thick) may then be sputtered on the substrate and patterned to help with the initialization of the machining process. It can be skipped when using a low resistivity Si substrate. High-aspect-ratio Si structures can be formed by any variety of high-aspect-ratio Si etching processes [33]. In this work, the Bosch process is performed on a STS Pegasus DRIE tool (Surface Technology Systems, United Kingdom, now part of SPP Process Technology Systems Ltd). This process alternates etching and passivation steps for highly anisotropic etching of Si. In the etching step, SF_6 plasma anisotropically attacks the exposed Si, while in the passivation step, C_4F_8 gas is used to create a protective polymer film [33]. After the Si microstructures are formed, an adhesion layer of Ti film of 10–20 nm thickness and an Au film of 200–500 nm thickness are evaporated on the backside of the Si wafer to help form low-resistance Ohmic contact between the Si tool and the μEDM discharge circuit. The wafer can then be diced into desired die sizes for use as cutting tools in batch mode μEDM.

The Si tool die is then installed into the SmalTec™ EM203 μEDM machine for batch mode μEDM. A schematic drawing of this equipment, along with the customization for batch mode μEDM, is shown in figure 2. The equipment can generate discharges with energy levels <100 nJ. The built-in *XYZ* motorized stages have 0.1 μm resolution [34]. The *Z* stage drives the cutting tool and provides the feeding motion during machining. The *X–Y* stages move the workpiece that is mounted on a worktable.

Batch mode μEDM is performed with machining control parameters developed according to desired machining conditions. These parameters include discharge voltage and capacitance, *Z*-stage feeding rate, and a set of parameters

that determine the *Z*-stage motion pattern when short-circuit events occur. With proper selection of these parameters, the machining rate can be optimized for the desired feature geometry and dimension.

Debris generated in the μEDM process include particles removed from the workpiece and the tool, as well as carbon residue from the dielectric oil [20]. If not efficiently removed, the debris can accumulate between the tool and the workpiece. This can cause excessive secondary discharges and short-circuit events, slowing down or even prematurely stopping the machining. A secondary discharge is an undesirable discharge between the cutting tool and debris, or between the workpiece and debris. A short-circuit event is an undesirable short circuit between the cutting tool and the workpiece, generally caused by direct physical contact, which prevents the initiation of a discharge.

Serial mode μEDM typically relies on spinning the axis-symmetric tool to efficiently remove debris. In batch mode μEDM, tool rotation is not an option, but alternatives are available. For example, the dielectric oil can be injected near the machining region, creating a flow to flush debris. Additionally, the metal workpiece can be mounted on a vibrator which provides a dithering vertical motion in the feeding (*Z*) direction of the cutting tool at a frequency of 100 Hz and adjustable amplitude to facilitate removal of machining debris. This vibration also helps to avoid micro-welding when a short circuit occurs between the tool and the workpiece. During the short-circuit events, the *Z*-stage retracts from the workpiece to break up the short circuit. The corresponding process control parameters define how the retraction is performed, including the distance, movement speed, discharge voltage status, etc. With proper selection of these parameters, a plunging motion can be triggered each time when there is a short-circuit event, to quickly squeeze dielectric oil out of the machined cavities on the workpiece, carrying along the accumulated debris in the gap.

2.3. Optional sidewall passivation coating for tools with $\leqslant$10 μm features

As noted above, the debris that is present in the discharge gap can initiate secondary discharge on the sidewalls and the base of the tool electrode during the machining process. For electroplated copper tools, this can cause excessive heating and recasting of the tool features into a mushroom shape. The debris can also become locally welded to both the workpiece and the tool after excessive accumulation and significant amount of spurious discharges [20]. A technique that adds an insulating layer on the sidewalls and base of the copper tools has been reported to reduce spurious discharges. A thin layer of sputtered Si is used for this purpose and discharges occur preferentially at the top of the tool which has the path of the least resistance [35].

For Si tools, softening and recasting is not as much a concern given its higher melting point and absence of a softening temperature. However, erosion on the sidewalls of the tool caused by spurious discharges can still be a serious issue especially for tools with wall thickness of $<$10 μm, causing premature damage of the tool structures. This issue is further compounded by the already-existing potential of damage from the local pressure fluctuations or shock waves formed in the dielectric oil due to the released heat from the discharges. Sidewall passivation coating for such tools can protect the sidewalls from spurious discharges while allowing machining discharges to occur mainly from the top of the tool structures.

A process sequence for the preparation of Si tools with SiO_2 passivation coating on the sidewalls and the base is shown as option 2 in figure 1. The process is adapted from the local oxidation of silicon process for CMOS transistor fabrication [36]. It starts with low-pressure chemical vapor deposition (LPCVD) of a silicon nitride film on a p^{++} Si substrate. The nitride film is patterned by reactive ion etching (RIE), which is followed by DRIE of the bulk Si to form the high-aspect-ratio tool structures. Thermal oxidation of Si is then performed to grow a SiO_2 layer of selected thickness. The surfaces covered by the nitride film, including the top of the tool structures, have no SiO_2 grown. After oxidation, the nitride film is removed by hot phosphorus acid etching. Finally Ti/Au thin films are deposited on the backside of the wafer for electrical contact, and the wafer can be cut into smaller sizes for machining use.

3. Process characterization

The batch mode μEDM process using DRIE Si tools has been experimentally validated for several workpiece materials, including SS304, SS316, and titanium (Grade 1). The two types of stainless steel, SS304 and SS316, are examples of the most widely used stainless steel varieties. Both types have chromium and nickel content. Titanium (Grade 1) is unalloyed titanium with low oxygen composition. This is used as an example of the many varieties in the titanium/titanium alloy material category. The material properties and E_I index for SS304 and Ti (Grade 1) are listed in table 1. Machining characteristics such as machining rates, tool wear ratios and machining uniformity are derived.

3.1. Fabrication of silicon tools with/without sidewall passivation

For process characterization, 5 $\times$ 5 mm^2 Si tools were prepared with various tool structures formed by DRIE, including features representing straight and curved channel arrays, round and square cavity arrays, cross channel array, etc. Three example tool structures, Si1–Si3, are shown in figure 3 and summarized in table 2. The initial p^{++} Si wafer has a thickness of $\approx$550 μm.

The first two tool structures shown in figure 3, Si1 and Si2, are examples of bare Si tools without SiO_2 coating. These structures have a height of 90 $\pm$ 3 μm and a minimum lateral feature size of 5 μm, giving an aspect ratio up to 18. The etching time for DRIE was 20 min, giving an etching rate of $\approx$4.5 μm min^{-1} for the heavily boron-doped silicon. The Ti/Au coating on the backside has thicknesses of 20 nm/400 nm. This thin film metal layer helps reduce the contact resistance to the p^{++} Si die to $<$5 Ω from typical values of 200–2000 Ω without the layer.

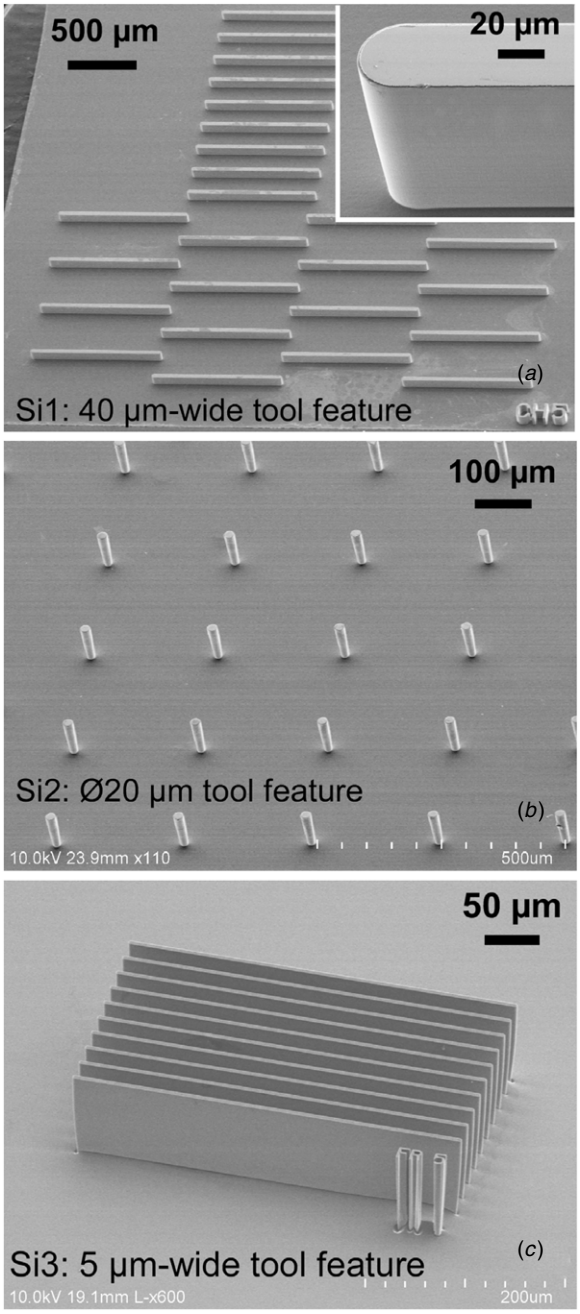

Figure 3. SEM images of three of the 5 × 5 mm^2 Si tool dies with high-aspect-ratio structures. (*a*) Bare Si tool for array of straight channel segments, 40 μm wide, 1 mm long. (*b*) Bare Si tool for 17 × 17 array of Φ20 μm holes. (*c*) Si tool with SiO_2 sidewall coating, for array of straight channel segments, 5 μm wide, 400 μm long. Feature heights: (*a*) and (*b*) 90 ± 3 μm; (*c*) 105 ± 3 μm.

The structure shown in figure 3(*c*) is an example of the Si tools with SiO_2 passivation coating on the sidewalls. During the fabrication, a low-stress LPCVD nitride film with a thickness of ≈150 nm was used for oxidation masking. The use of low-stress nitride film eliminates the need of a pad oxide layer underneath [36]. Regarding the minimum thickness necessary for the SiO_2 passivation layer, the breakdown field in thermal oxides (>1 × 10^7 V cm^{-1}) is considered to generate a preliminary estimation. For a discharge voltage up to 100 V, the SiO_2 layer needs a thickness >100 nm. The final SiO_2 thickness on the tool sidewalls was varied in the range from 180 to 530 nm in different batches of fabrication. The final structures have a height of 105 ± 3 μm, providing an aspect ratio up to 21.

Table 2. Summary of three example structures formed on 5 × 5 mm^2 Si tools and their resulting workpiece characteristics.

Tool label	Workpiece label	Workpiece characteristics	Feature
Si1	SS1	Line width: 52 μm; length: 1 mm; spacing: 250 μm/500 μm	
Si2	SS2	Diameter: 26 μm; spacing: 250 μm; 17 × 17 array	
Si3	SS3	Line width: ⩾7 μm; length: 400 μm; spacing: 25 μm	

Table 3. Selected machining parameters for batch mode μEDM with DRIE Si tools.

Discharge voltage	50–80 V
Discharge control capacitance	10–100 pF
Tool die size	5 × 5 mm^2
Max. machining rate (in feature depth) demonstrated	≈5 μm min^{-1}
Min. feature size demonstrated	≈7 μm
Discharge gap (vary with discharge energy, etc)	1–6 μm
Max. aspect ratio demonstrated	3.2
Typical sidewall angle	87°–89°
Workpiece surface roughness	120/126 (SS304)
R_a pre/post-machining (nm)	8/121 (Ti-Grade 1)
Tool wear ratio	1 ± 0.3
Stage dithering	≈15 μm at 100 Hz

3.2. Machining of SS304 without tool sidewall passivation

The batch mode μEDM process with DRIE Si tools is evaluated on SS304 substrates. The tools were mounted on the custom electrode holder using conductive epoxy for preliminary implementation. Multiple sets of machining control parameters for batch mode μEDM were investigated to accommodate different machining situations caused by variations in feature geometry and dimension. For fine features at the micro-scale, a low discharge voltage of 50–80 V was used with a discharge control capacitance in the range of 10–100 pF. The machining rate, defined as the cutting depth per unit time, is typically affected by the settings of the control parameters. These have been optimized for each type of geometry and dimension range in the experiments to minimize the portion of time in idle, approaching, or retraction (due to short circuit), thus maximizing the portion of time in active discharge/machining. Selected machining parameters and characteristics are summarized in table 3.

The test patterns were successfully transferred onto SS304 substrates, confirming the feasibility of using Si cutting tools for batch mode μEDM. Figure 4 shows the channel-array pattern that is defined on the cutting tool Si1 (figure 3(*a*))

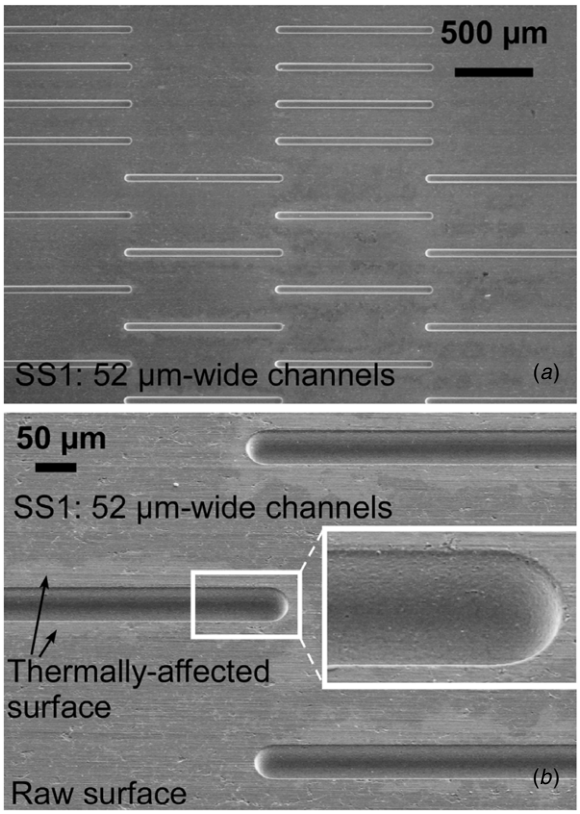

Figure 4. SEM images of array of 52 μm wide 1 mm long straight channel segments formed on SS304 substrate, using the Si1 tool shown in figure (*a*). Discharge gap: ≈6 μm; channel depth: ≈32 μm; machining rate: ≈5 μm min^{-1}. (*a*) Top–down view; (*b*) perspective view with insert showing close-up details.

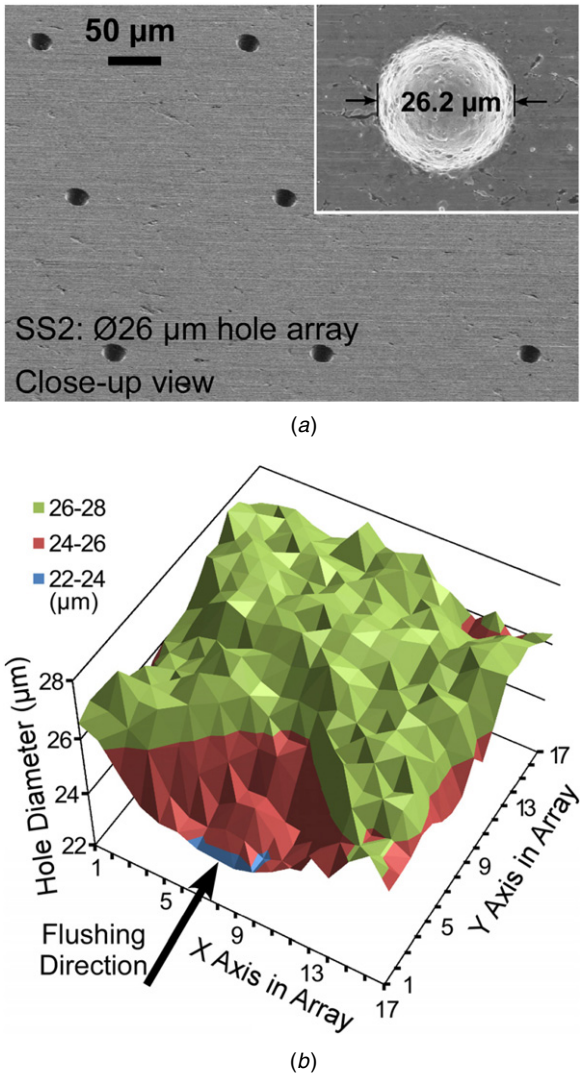

Figure 5. (*a*) SEM images of 17 × 17 array of Φ26 μm holes made on SS304 substrate, using the Si2 tool shown in figure 3(*b*). Discharge gap: ≈3 μm; hole depth: ≈22 μm; machining rate: ≈3 μm min^{-1}. Markings on the SS304 surface are from raw material. (*b*) Diameter variation of the Φ26 μm holes in the 17 × 17 array. Mean hole diameter: 26.5 μm. Standard deviation: 0.97 μm. Range: 23.8–27.7 μm. Flushing helps remove debris and reduce discharge gap, thus smaller holes closer to the flushing spout.

and transferred onto SS304. The tool structure has a width of 40 μm and a length of 1 mm each. After μEDM, the channel width becomes 52 μm due to a discharge gap of ≈6 μm. The depth of the machined channels is ≈32 μm with a machining time of ≈6 min, giving a machining rate of ≈5 μm min^{-1}. Figure 4(*b*) shows the close-up view and the thermally-affected surfaces with color change beside the machined channels. The lateral extension of the thermally-affected surfaces beyond the machined features is caused by accumulated debris, and the resulting weaker secondary discharges that generate heat. However, the impact is insufficient to remove the workpiece material.

Figure 5(*a*) shows a 17 × 17 array of round cavities formed on SS304 using the Si2 tool pattern shown in figure 3(*b*). The 20 μm tool diameter becomes the 26 μm hole diameter on the workpiece, indicating a discharge gap of ≈3 μm. The cavity depth is ≈22 μm with a machining rate of ≈3 μm min^{-1}. Figure 5(*b*) plots the cavity diameter distribution for this 17 × 17 array of holes. The cavity diameter has a standard deviation of 0.97 μm and a mean diameter of 26.5 μm. Because the flushing motion of dielectric oil helps remove debris from the machining region and thus reduce discharge gap, cavities with smaller diameters are located closer to the flushing spout, where flushing is the most effective. A similar pattern of 17 × 17 array of 49 μm diameter holes is machined through a 30 μm thick SS304 foil (figure 6). The tool used for this pattern has hole spacing of 250 μm and hole diameter of 40 μm, indicating a discharge gap of 4.5 μm. The hole diameters on the exit side of the SS304 foil are 1–3 μm smaller than on the entrance side, giving an almost vertical sidewall with an angle of ≈87°–89°. This angle can be further improved toward 90° by further feeding the tool deeper into the workpiece after the workpiece has been cut through.

The wear ratio of the tool is given by the ratio of the tool volume worn to the workpiece volume removed [11]; in batch mode μEDM, this is approximately equivalent to the ratio of the tool height worn to the machined depth on the workpiece. The wear ratio depends on many factors, including discharge energy and polarity, materials involved in discharges, effectiveness of debris removal, feature geometry and density, etc. For Si tools with the demonstrated machining

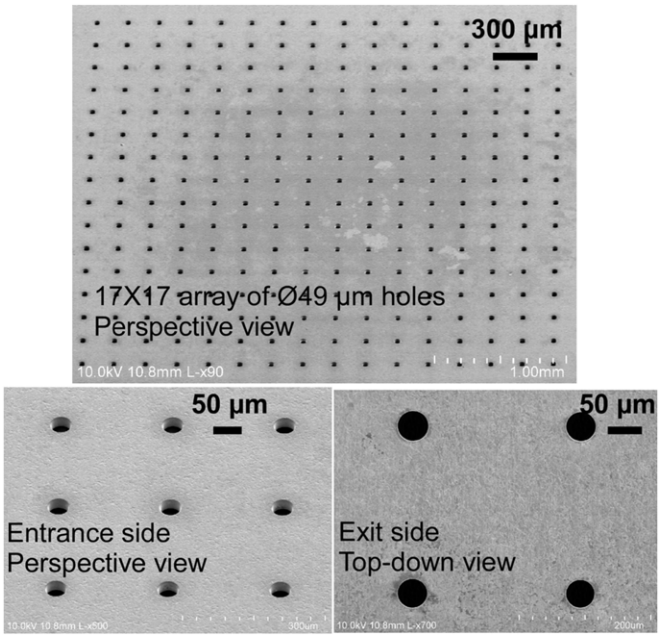

Figure 6. SEM images of 17 × 17 array of Φ49 μm holes machined through a 30 μm thick SS304 foil. Discharge gap: ≈4.5 μm. The bottom two images show the close-up view on the entrance and exit sides of the foil. The hole diameters on the exit side are 1–2 μm smaller than on the entrance side, indicating an almost vertical sidewall angle of ≈88°–89°.

conditions and patterns, the typical wear ratio is 1 ± 0.3 when the tool features have a lateral thickness of more than a few microns. Figure 7(*a*) shows a Si tool Si1 after being used for machining a SS1 pattern of ≈15 μm depth. The tool wear ratio is ≈0.9. For comparison, figure 7(*b*) provides a previous result that shows a post-use electroplated Cu tool without any coating on the sidewalls [35]. It is notable that the mushroom-shaped recast top present in the uncoated Cu tool does not appear in the Si tool. For tool features with a lateral wall thickness of a few microns, such as that shown in figure 3(*c*), the tool structures are weakened by secondary discharges on the sidewalls and are prone to premature damage by the thermal shock waves during the machining. Thus, the machined depth of such features using uncoated Si tools are generally limited to <5 μm, typically accompanied by a total loss of the tool structures. For features with lateral dimensions ⩽10 μm, superior machining results are obtained with protected tool sidewalls as described below.

3.3. Machining of ⩽10 μm features using tools with sidewall passivation

To fabricate the feature sizes of 10 μm or smaller using Si tools, the lateral thickness of the tool structures is further reduced to a few microns due to the discharge gap on both sides of the tool. A SiO_2 layer for passivation and protection of the tool sidewalls is used for these tools, as well as other tools with larger feature sizes, to assess the effect of this coating layer on the μEDM process.

Figure 8(*a*) shows an array of straight channels, each with a width of ≈10 μm and length of 400 μm, formed on a SS304 substrate. These were made using the Si3 tool

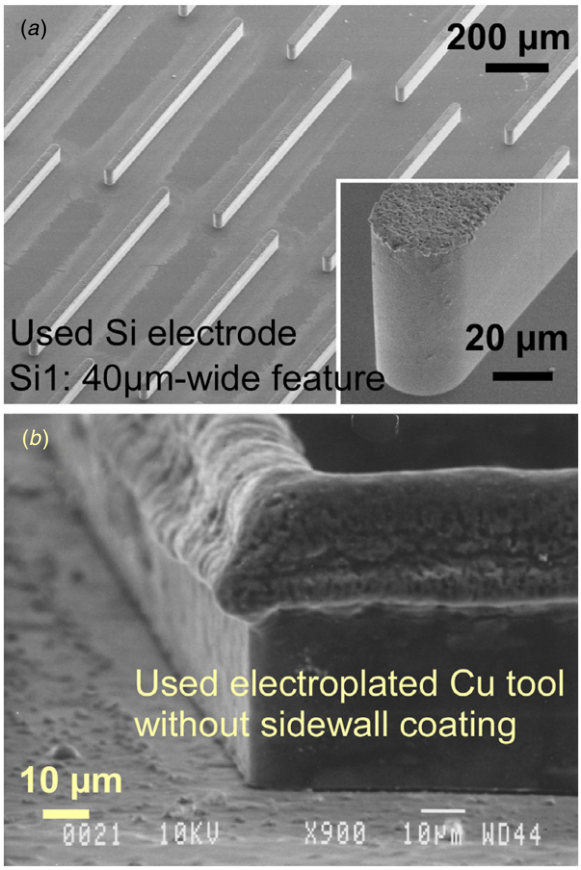

Figure 7. (*a*) SEM images of the Si tool shown in figure 3(*a*) after being used for machining. The insert shows close-up details. (*b*) Previous result showing post-use electroplated Cu tool without any coating, for comparison. Note the mushroom-shaped recast top in the uncoated Cu tool does not appear in the Si tool.

shown in figure 3(*c*) with a tool width of 5 μm and spacing of 25 μm. The discharge gap is ≈2.5 μm and the channel depth is ≈28 μm, giving an aspect ratio of 2.8. The machining rate is ≈0.8 μm min^{-1}. The machined depth, and thus, the aspect ratio, are significantly improved from those using uncoated Si tools. As shown in figure 8(*b*), the tool structures remain intact except for the regular wear, while the uncoated tools with the same geometry were totally lost during the machining of much shallower channels. The wear ratio of the example shown in figure 8(*b*) is ≈1.0, comparable to the values of other larger uncoated tools. One issue that is under investigation is that the SiO_2 layer on the sidewalls appears to have peeled off near the top portion of the tool structure during machining. SiO_2 coatings of multiple thicknesses in the range of 180–530 nm were tested and similar results were obtained. The actual mechanism for the peel-off is uncertain, though it may be related to the thermal stress generated during the machining. When the thickness of the SiO_2 is larger (530 nm), the machining rate noticeably slows down, which is likely related to the reduction in the proportion of surface area at the tool top available for active discharges.

Figure 8(*c*) shows the variation of average measured discharge gap as a function of the discharge energy used for machining under otherwise identical machining conditions. The tool pattern was Si3 and a set of machining tests were

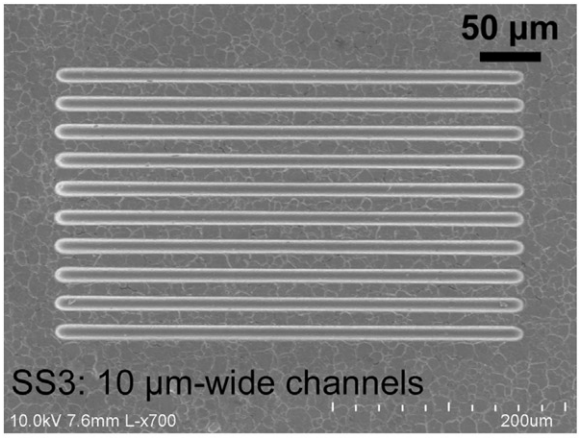

(*a*)

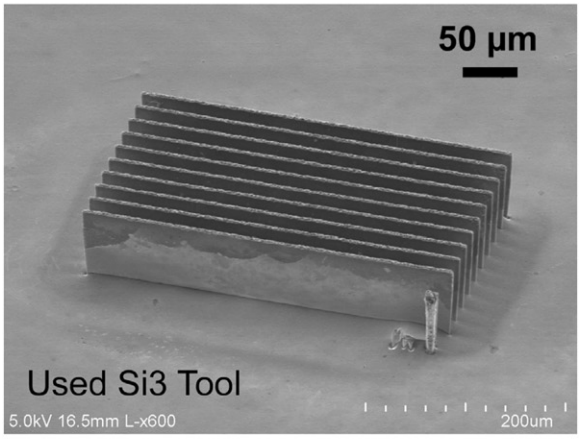

(*b*)

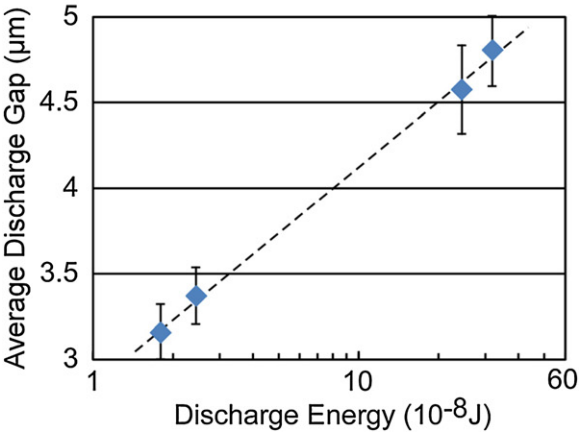

(*c*)

Figure 8. (*a*) SEM image of ≈10 μm wide, 400 μm long straight channel segments formed on SS304 substrate, using the Si3 tool shown in figure 3(*c*). Discharge gap: ≈2.5 μm; channel depth: ≈28 μm; aspect ratio: 2.8; machining rate: ≈0.8 μm min^{-1}. The texture on the SS304 surface is from the raw material. (*b*) SEM image of one of the used Si3 tools. Tool wear ratio: ≈1.0. (*c*) The variation of average measured discharge gap as a function of the discharge energy used for machining under otherwise identical machining conditions. An approximate exponential relationship is shown. The error bars are one standard deviation from the mean values ($n = 8$).

performed on the same SS304 substrate. The discharge energy (E) is:

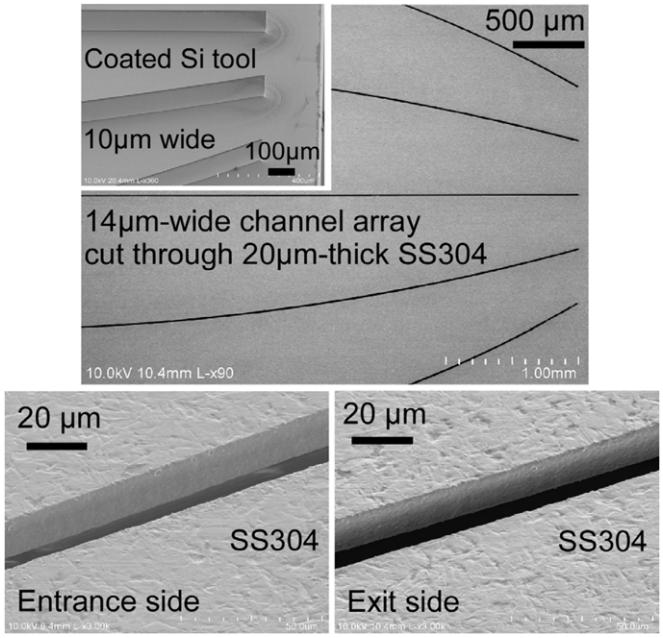

Figure 9. SEM images of ≈14 μm wide, >4.5 mm long curved channel segments formed through a 20 μm thick SS304 foil. Discharge gap: ≈2.0 μm. Variation of channel width between the entrance and the exit sides: 1–2 μm. Sidewall angle: ≈87°–88°.

$$E = \tfrac{1}{2}CV^2 \tag{2}$$

where C is the discharge control capacitance and V is the discharge voltage between the tool and the workpiece. The value of C is varied between two options: 10 and 100 pF, while the value of V is changed among 60, 70, and 80 V. As shown in the figure, an approximate exponential relationship appears according to the dashed trend line. The fabricated features with different discharge energy have similar machined depth; however, the tool wear and surface roughness tend to degrade with larger discharge energy, consistent with the description in [17].

Other typical microfluidic structures with various feature sizes were also evaluated. The machining characteristics for larger feature sizes are typically similar to those using uncoated Si tools. As one such example, shown in figure 9 is an array of curved channels with ≈14 μm width and >4.5 mm length formed through a 20 μm thick SS304 foil. The feature width on the SiO_2 coated tool is 10 μm, indicating a discharge gap of ≈2.0 μm. The variation of the channel width between the entrance and the exit sides is 1–2 μm, giving a machined sidewall that is approximately vertical and an angle of 87°–88°.

3.4. Machining of other workpiece materials

Other workpiece materials have also been tested for batch mode μEDM with Si tools, such as titanium (Grade 1) and SS316. As shown in table 1, the listed material properties of Ti (Grade 1) are very similar to those of SS304, thus an almost identical E_I index and similar machining performance during EDM. The machining characterization results on Ti (Grade 1) match this prediction pretty well. Figure 10 shows the curved

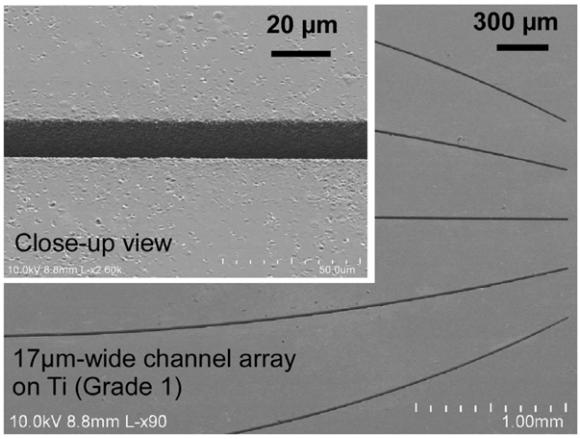

Figure 10. SEM images of ≈17 μm wide, >4.5 mm long curved channel segments formed on a Ti (Grade 1) substrate. Discharge gap: ≈3.5 μm; machined depth: ≈55 μm; aspect ratio: ≈3.2; machining rate: ≈2 μm min^{-1}.

channel segments formed on a Ti (Grade 1) substrate with ≈17 μm width and >4.5 mm length. The pattern was formed using an uncoated Si tool with a tool width of 10 μm. The discharge gap is ≈3.5 μm. The machined depth is ≈55 μm with a machining time of 27 min, giving an aspect ratio of ≈3.2 and a machining rate of ≈2 μm min^{-1}. As can be seen in the image, the mirror surface of the raw Ti substrate is attacked by the accumulated debris during μEDM and the surface finish is degraded. Measurement of the roughness R_a reveals that the average roughness value degrades from ≈8 nm on the virgin surface to ≈121 nm on the attacked surfaces. This attack is less obvious on SS304 as the virgin surface already has comparable roughness to the machined surfaces (table 3). The machining results on SS316 are also similar to that of SS304, though the machined surface finish tends to be rougher.

Titanium (Grade 1) and SS316 are examples of other workpiece materials that can be processed by batch mode μEDM. The observed machining performance is similar to those of SS304 as summarized in table 3, which is not surprising given the comparable thermal material properties. In general, μEDM can be performed on any electrically conductive material, with variation in machining rate, tool wear and other characteristics corresponding to different material properties of the workpiece.

4. Discussion

During batch mode μEDM, the actual machining rate is reduced from the nominal rate at which the Z stage is advanced by short-circuit events occurring between the tool and the workpiece, as well as by the short circuits or secondary discharges between these components and the debris. These occurrences are normal to the μEDM process. To achieve faster machining rates, higher discharge energy can be used at the expense of achievable minimum feature size and surface quality.

For fine and closely-spaced features, effective debris removal from the gaps between the tool and the workpiece is essential for rapid machining and uniformity. Debris removal can be performed using any combination of the techniques identified in section 2.2, including effective oil flushing, worktable dithering and specially-designed control parameters for Z-stage retraction. The simultaneous use of these techniques typically provides the best results. Debris removal can also be further facilitated by hydrodynamic flushing. This can be done using a two-step machining method [35]. In the first step, narrow through-holes are formed in the workpiece; these become a path for debris to escape from the machining gap in the second step. Alternatively, through-holes for debris flushing can be integrated into the tool substrate if the pattern design allows. This technique was previously shown to help improve feature geometry quality and reduce tool wear in batch mode μEDM with electroplated Cu tools [35]. However, special tools and/or through holes on the workpiece are necessary and may not be feasible depending on the machining requirements.

The minimum feature size (L_m) that can be achieved in batch mode μEDM is given by:

$$L_m = T_m + 2D_g \tag{3}$$

where T_m is the feature size of the tools and D_g is the discharge gap. For Si tools made by DRIE with high-aspect-ratio positive structures, a feature size of 1–2 μm can be readily achieved with an aspect ratio >10 [33]. The discharge gap mainly relies on the amount of discharge energy but can also be affected by other factors such as debris removal effectiveness, etc. Typically a minimum value of 1–2 μm can be obtained. Given these, a minimum feature size L_m of 3–5 μm is likely the limit. In this work, minimum feature size of ≈7 μm has been obtained with tools of 5 μm feature size. This may be further reduced by using smaller tool features and lower discharge energy.

The wear ratio of the Si tools is typically in the range of 1 ± 0.3. This means that for every 1 μm of machined depth on the workpiece, 0.7–1.3 μm tool height is worn away. This tool wear can be compensated by increasing the height of the Si microstructures, which can be readily achieved considering the capability of mature DRIE technology. The die-scale tools can also be readily replaced as these can be mass manufactured at the wafer scale. Tailoring of the thermal and electrical characteristics of the sidewall coating may further improve the tool wear ratio; this will be investigated in future effort.

In this work, the machining process has been demonstrated at the die scale. For wafer-scale manufacturing, certain equipment modifications and enhancement are anticipated. These include mechanisms to correct the curvatures of the tool wafer and the workpiece while maintaining the flatness and parallelism of both. Debris removal also becomes more challenging at the larger scale, and hydrodynamic flushing using tools with built-in debris exits may be needed to remove debris from the center region of the wafer. The simultaneous allowance of multiple discharges may also be needed for higher throughput during batch mode μEDM at the wafer scale [17]. In this, the tool structures are electrically partitioned into multiple groups; each group is connected to a separate discharge circuit, thus allowing simultaneous initiation of discharges and machining with each group.

5. Conclusions

The feasibility and mechanism of using DRIE Si cutting tools in batch mode μEDM have been verified and the process characteristics have been assessed. The machining process has been successfully demonstrated on SS304, SS316 and Ti (Grade 1) with various feature geometries (channels and cavities) and dimensions ($\geqslant$7 μm). Aspect ratios up to 3.2 and machining rates up to $\approx$5 μm min^{-1}. have been achieved. For machining of ultra-fine features with sizes $\leqslant$10 μm, a process sequence has been described for preparation of Si tools with SiO_2 coatings to passivate and protect the tool sidewalls from spurious discharges. The effectiveness of the coated Si tools has been verified. These experiments substantiate the potential of the process for a variety of applications, which will be pursued in future effort.

Acknowledgments

The research effort was supported in part by a gift fund from Agilent Research Laboratories. Facilities used for this research include the Lurie Nanofabrication Facility (LNF) operated by the Solid-State Electronics Laboratory (SSEL) at the University of Michigan.

References

[1] Takahata K, Gianchandani Y B and Wise K D 2006 Micromachined antenna stents and cuffs for monitoring intraluminal pressure and flow *J. Microelectromech. Syst.* **15** 1289–98

[2] Ko W H 1995 Packaging of microfabricated devices and systems *Mater. Chem. Phys.* **42** 169–75

[3] Quimby B D, McCurry J D and Norman W M 2007 Capillary flow technology for gas chromatography: reinvigorating a mature analytical discipline *LCGC North America* (www.chem.agilent.com/cag/prod/GC/LCGC_Article.pdf)

[4] Ozkeskin F M, Sangjo C, Sarabandi K and Gianchandani Y B 2012 An all-metal micro-relay with bulk foil Pt-Rh contacts for high-power RF applications *IEEE Trans. Microw. Theory Tech.* **60** 1595–604

[5] Wright S A, Harvey H Z and Gianchandani Y B 2013 A microdischarge-based deflecting-cathode pressure sensor in a ceramic package *J. Microelectromech. Syst.* **22** 80–86

[6] Li T, Ding K, Seyfried W E and Gianchandani Y B 2012 A micromachined chemical sensor for sea floor environments: initial results *Hilton Head 2012: Solid State Sensor, Actuator and Microsystems Workshop (Hilton Head Island, SC)* pp 173–6

[7] Zhang X and Li X 2010 Design and characterization of thin-film system for microsensors embedding in Ti6Al4V alloys *IEEE Sensors J.* **10** 839–46

[8] Brunette D M, Tengvall P, Textor M and Thomsen P 2001 *Titanium in Medicine: Material Science, Surface Science, Engineering, Biological Responses and Medical Applications* (Berlin: Springer)

[9] Siegel G 2002 Anti-theft element *US Patent Specification* 6348865B1

[10] Viswanath A, Green S R, Kosel J and Gianchandani Y B 2013 Metglas-Elgiloy bi-layer, stent cell resonators for wireless monitoring of viscosity and mass loading *J. Micromech. Microeng.* **23** 025010

[11] Reinecke H and Muller C 2008 Micromachining *Comprehensive Microsystems* vol 1 ed Y B Gianchandani, O Tabata and H Zappe (Amsterdam: Elsevier) pp 379–402

[12] Nowak R and Metev S 1996 Thermochemical laser etching of stainless steel and titanium in liquids *Appl. Phys.* A **63** 133–8

[13] Kim B H, Ryu S H, Choi D K and Chu C N 2005 Micro electrochemical milling *J. Micromech. Microeng.* **15** 124–9

[14] Rao P N and Kunzru D 2007 Fabrication of microchannels on stainless steel by wet chemical etching *J. Micromech. Microeng.* **17** N99–106

[15] Masaki T, Kawata K and Masuzawa T 1990 Micro electro-discharge machining and its applications *Proc. IEEE Micro Electro Mechanical Systems: An Investigation of Micro Structures, Sensors, Actuators, Machines and Robots (Napa Valley, CA)* pp 21–26

[16] Pham D T, Dimov S S, Bigot S, Ivanov A and Popov K 2004 Micro-EDM—recent developments and research issues *J. Mater. Process. Technol.* **149** 50–57

[17] Takahata K and Gianchandani Y B 2002 Batch mode micro-electro-discharge machining *J. Microelectromech. Syst.* **11** 102–10

[18] Guckel H 1998 High-aspect-ratio micromachining via deep x-ray lithography *Proc. IEEE* **86** 1586–93

[19] Kao Y L, Tu G C, Huang C A and Chang J H 2004 The annealing behavior of copper deposit electroplated in sulfuric acid bath with various concentrations of thiourea *Mater. Sci. Eng.* A **382** 104–11

[20] Takahata K 2005 Batch manufacturing technology based on micro-electro-discharge machining and application to cardiovascular stents *PhD Thesis* University of Michigan, Ann Arbor, MI, USA

[21] Takahata K, Shibaike N and Guckel H 1999 A novel micro electro-discharge machining method using electrodes fabricated by the LIGA process *MEMS' 99: Proc. IEEE Int. Conf. on Micro Electro Mechanical Systems (Orlando, FL)* pp 238–43

[22] Takahata K, Shibaike N and Guckel H 2000 High-aspect-ratio WC–Co microstructure produced by the combination of LIGA and micro-EDM *Microsyst. Technol.* **6** 175–8

[23] Kim B H, Park B J and Chu C N 2006 Fabrication of multiple electrodes by reverse EDM and their application in micro ECM *J. Micromech. Microeng.* **16** 843–50

[24] Zeng W, Wang Z, Weng M and Liu Y 2012 Micro-electrode array and micro-hole array fabrication by combined micro-WEDM and EMM *Digest J. Nanomater. Biostruct.* **7** 755–61

[25] Kuo C-L and Huang J-D 2004 Fabrication of series-pattern micro-disk electrode and its application in machining micro-slit of less than 10 μm *Int. J. Mach. Tools Manuf.* **44** 545–53

[26] Li T, Bai Q and Gianchandani Y B 2012 Using DRIE silicon as a cutting tool for high precision micromachining of metal alloys *Hilton Head 2012: Solid State Sensor, Actuator and Microsystems Workshop (Hilton Head Island, SC)* pp 477–80

[27] Gianchandani Y B and Takahata K 2003 Micro-electro-discharge machining utilizing semiconductor electrodes *US Patent Specification* 6586699B1

[28] Drozda T J and Wick C 1983 *Tool and Manufacturing Engineers Handbook: Machining* vol 1 4th edn (Dearborn, MI: Society of Manufacturing Engineers)

[29] Kruth J-P 1993 *Non-Conventional Machining Technologies: Part I* (Leuven: VTK) (in Dutch)

[30] Reynaerts D, Heeren P-H s and Van Brussel H 1997 Microstructuring of silicon by electro-discharge machining (EDM)—part I. Theory *Sensors Actuators* A **60** 212–8

[31] Moylan S P, Chandrasekar S and Benavides G L 2005 High-speed micro-electro-discharge machining *Sandia*

Report SAND2005-5023 (Oak Ridge, TN: United States Department of Energy)
[32] Mahendran S, Devarajan R, Nagarajan T and Majdi A 2010 A review of micro-EDM *IMECS'10: Proc. Int. MultiConf. of Engineers and Computer Scientists (Hong Kong)* vol 2
[33] Wu B, Kumar A and Pamarthy S 2010 High aspect ratio silicon etch: a review *J. Appl. Phys.* **108** 051101
[34] SmalTec LLC 2012 EM203 Micro EDM machine (www.smaltec.com/em203.cfm)
[35] Richardson M T and Gianchandani Y B 2008 Achieving precision in high density batch mode micro-electro-discharge machining *J. Micromech. Microeng.* **18** 015002
[36] Smeys P 1996 Geometry and stress effects in scaled integrated circuit isolation technologies *PhD Thesis* Stanford University
[37] Asheghi M, Kurabayashi K, Kasnavi R and Goodson K E 2002 Thermal conduction in doped single-crystal silicon films *J. Appl. Phys.* **91** 5079–88
[38] Ioffe Physico-Technical Institute 2012 New Semiconductor Materials—Characteristics and Properties www.ioffe.ru/SVA/NSM/Semicond/ Si/thermal.html
[39] McConnell A D and Goodson K E 2005 Thermal conduction in silicon micro- and nanostructures *Annu. Rev. Heat Transfer* **14** 129–68
[40] AZoM 2012 The A to Z of Materials www.azom.com/
[41] Chemicool 2012 The Periodic Table www.chemicool.com/
[42] eFunda 2012 Properties of Common Solid Materials www.efunda.com
[43] MatWeb 2012 MatWeb Material Property Data www.matweb.com